Check for updates

Received: 23 November 2020 | Revised: 3 May 2021 | Accepted: 26 May 2021
DOI: 10.1002/er.6937

RESEARCH ARTICLE

INTERNATIONAL JOURNAL OF ENERGY RESEARCH WILEY

Space degradation of triple junction solar cells at low temperatures: II-electron irradiation

Seonyong Park[1] | **Olivier Cavani**[2] | **Jérémie Lefèvre**[2] | **Carsten Baur**[3] | **Victor Khorenko**[4] | **Bruno Boizot**[5]

[1]Solar Array Department, Airbus Defence and Space GmbH, Taufkirchen, Germany
[2]Laboratoire des Solides Irradiés, CNRS-UMR 7642, CEA-DRF-IRAMIS, Ecole Polytechnique, Université Paris-Saclay, Palaiseau, France
[3]ESTEC, European Space Agency, Noordwijk, The Netherlands
[4]AZUR SPACE Solar Power GmbH, Heilbronn, Germany
[5]Service de Recherche en Métallurgie Physique, Université Paris-Saclay, CEA, Gif sur Yvette, France

Correspondence
Seonyong Park, Airbus Defence and Space GmbH, Willy-Messerschmitt-Strasse 1, 82024 Taufkirchen, Germany.
Email: seonyong.park@polytechnique.edu

Summary
We investigated the behavior of electron-irradiated 3G28 InGaP/GaAs/Ge triple junction solar cells and their component (top, middle and bottom) cells at low temperatures from 100 to 300 K and low illumination intensity. Significant degradation of their performances has been observed. We found that it is induced by an excess current associated with tunneling due to the presence of the radiation-induced defects introduced in the junctions of each sub-cell. The amount of tunneling current, hence of the effect of degradation, is significantly higher in the bottom sub-cell than in the top and middle sub-cells. This particular cell is formed by diffusion of group V atoms into p-Ge substrate, which leads to relatively inhomogeneous doping profile and thus tunneling current distribution compared to well controlled top and middle sub-cells deposited by epitaxy. The degradation associated with tunneling recovers significantly at 300 K in the bottom cell.

KEYWORDS
defect, electron irradiation, excess, lattice-matched GaInP/GaAs/Ge triple junction solar cell, low intensity low temperature (LILT), radiation induced trap assisted tunnelling

1 | INTRODUCTION

The aim of this work is to examine the behavior of state-of-the-art lattice matched GaInP/GaAs/Ge triple junction (TJ) 3G28 space solar cells from AZUR SPACE, under conditions of deep space (the so-called low intensity low temperature [LILT] conditions, for "Low Intensity of illumination and Low Temperature"). Solar cells degrade in space due to irradiation with high-energy particles, mostly electrons and protons. These particles produce lattice displacements, resulting in the creation of electrically active defects.[1-3] Some of these defects play the role of minority carriers traps, inducing a recombination of electron–hole pairs in the junctions,[4] thus, consequently decrease the cell performance.

Defect introduction is well studied for irradiations performed at room temperature (RT) for most of the materials currently used in the production of solar cells: Si,[5,6] GaAs,[7,8] GaInP,[9-12] and Ge,[13,14] . Information such as activation energy, structure, annealing temperature, capture cross section of some electrically active defects in these materials has been established. Systematic works for radiation on Si and GaAs solar cells, to understand and predict their electrical performance under the irradiation based on the defect information, have been done, too.[15] However, concerning low temperature (LT) irradiations, defect information mainly exists on material level for defects in GaAs,[7] to a lesser extent in Ge[16-19] and practically none in GaInP.

Meanwhile, as we discussed in the companion work dealing with proton radiation-induced degradation of the TJ solar cells,[20] the past studies of radiation effects in such cells have been limited to irradiation experiments

 © 2021 John Wiley & Sons Ltd.

performed around RT.[21-23] Extrapolations to LILT conditions were obtained by measuring RT-irradiated cells under LILT conditions,[24] with the exception of one attempt.[25] Preliminary results[26-28] seemed to suggest that the LT behavior of these cells does not depend on the irradiation temperature. However, recent observations showed that the degradation of TJ cells by electron irradiation is larger than expected[29,30] if it is only ascribed to the introduction of recombination centers by the irradiation, which should be temperature-independent process. These results also indicate that TJ cells after electron irradiation behave differently than after proton irradiation. Hence, we present here a detailed analysis of the electrical data acquired from electron-irradiated TJ cells and component cells following LT irradiation. It reveals several phenomena that have to be taken into account, such as dispersion of the end of life (EOL) performance of the electron-irradiated TJ cells under LILT condition, defect annealing, tunneling through radiation-induced defects in forbidden gap. These phenomena, in at least some of the component cells, are not present following RT irradiation. We therefore propose our interpretation by correlating the presented data and analysis with extensive literature studies.

2 | EXPERIMENTAL

The equipment used to perform LT irradiation with in situ current-voltage (*I–V*) measurements is the one described in the companion work.[20] The only difference is in the connection method between the electron accelerator and the cryostat chamber. 1-MeV electron irradiation was performed with two fluxes (half flux 2.5×10^{11} cm^{-2} s^{-1} and nominal flux 5×10^{11} cm^{-2} s^{-1}) and fluences varying from 1×10^{14} cm^{-2} to 3×10^{15} cm^{-2}. A half of the samples per fluence were irradiated with the half flux. Since no flux-related dependence was observed in this flux range, we do not classify the data by flux any longer. The beamline of the electron accelerator is separated from the cryostat chamber by a thin stainless-steel foil (see Figure 1) to keep the beamline under ultrahigh vacuum conditions. Thickness of the stainless- steel foil is 250 μm. Thus, the energy loss of 1 MeV electrons through this foil is about 20 keV which is negligible. Once the electrons penetrate the foil, they are scattered in the chamber. As a result, the current density depends on distance of the sample from the point where the scattering starts. To calibrate the fluence, we simply replaced the cell by a thick copper plate having the same area with the cell and directly measured the collected current. By monitoring the current from the accelerator control center, the current collected at the cryostat chamber (Faraday cup) and the current measured from the cupper plate, the ratio of these three current levels can be obtained. As a consequence, when irradiating solar cells, it is possible to indirectly measure the current that arrives to the cell.

Current-voltage (*I-V*) measurements in dark and under illumination have been carried out in-situ, that is, with the cell inside the cryostat chamber. The solar simulator, used with an illumination of 0.037 AM0 (≈ 50.5 W/m^2), is described by Khorenko et al.[31] The measurement set-up and the cryostat chamber are located in the radiation room where the electron beamline ends. For this reason, during the irradiation, test operator must not be present in the radiation room to avoid an exposure to very high level of radiation. first measurement can be performed around 2 minutes after irradiation is complete due to the following reasons: (a) to cool down the solar cell temperature heated by electron irradiation, (b) to

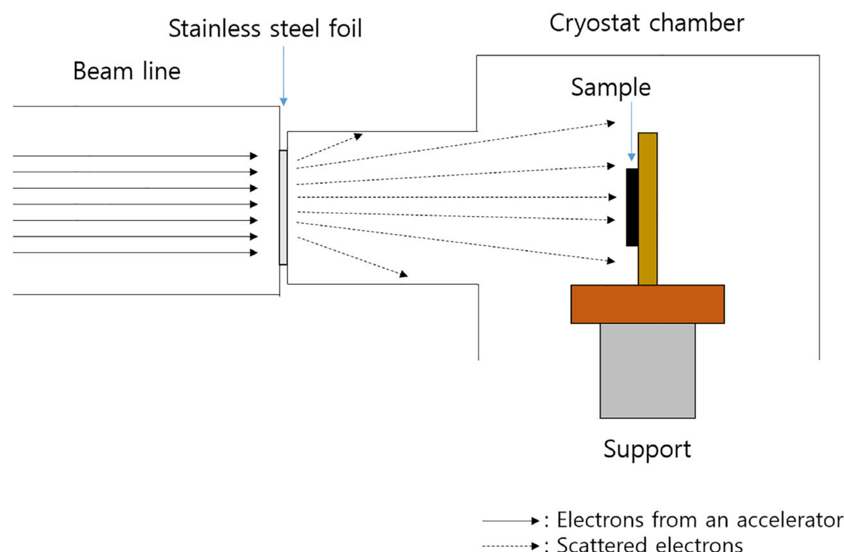

FIGURE 1 Diagram of the connection between the beamline of the linear electron accelerator and the cryostat chamber [Colour figure can be viewed at wileyonlinelibrary.com]

drop the radiation dose level in the radiation room down to the safe dose level. The measurement must still be performed as fast as possible to avoid any unwanted annealing at low temperature.

Typical *I–V* measurement in dark and under illumination was applied to the TJ cells and its component cells at temperatures ranging from 123 to 300 K. Hereby, a component cell is a cell which has the same optical structure as the TJ cell but in which only one sub-cell is electrically active among the three sub-cells.[20] LT irradiations for 2 cm x 2 cm TJ bare cells were conducted with different fluences: 7.5×10^{14} cm^{-2} (12 cells), 1.5×10^{15} cm^{-2} (24 cells), 3×10^{15} cm^{-2} (12 cells). Note that all electron-irradiated TJ cells are from the same batch. Once the cells were irradiated, *I–V* measurements were taken every 5 minutes to check until the stabilization of the EOL performance. These repetitive measurements were carried out during 30 minutes which was found to be a time after which no further change in electrical performance was detected. In this work, the EOL values taken after this step are labeled as LT annealed. Once cells have been heated up to 300 K and remeasured at low temperatures they are labelled as RT annealed.

Some of the TJ cells were irradiated at RT to be compared with the result of LT irradiation. In addition, top, middle and bottom component cells were cumulatively irradiated with 1 MeV electron fluences up to 3×10^{15} cm^{-2} at (100, 123, 200, 300) K. Moreover, isochronal annealing from 96 to 300 K was performed for the top and bottom component cells after irradiation at 96 K with intermediate measurements of the electrical parameters.

3 | RESULTS

3.1 | Irradiation of TJ cells

We present here BOL (beginning of Life = not irradiated) and EOL *I-V* characteristics in dark (DIV) and under illumination (LIV) of 3G28 TJ cells irradiated and measured at 123 K, comparing them with others irradiated and measured at 300 K.

Figure 2 shows an example of BOL and EOL LIV and PV curve of a cell irradiated at 123 K with a fluence of 3×10^{15} cm^{-2}, measured at 123 and 300 K.

The corresponding photovoltaic parameters are given in Table 1. At 123 K, short-circuit current (I_{SC}) value did not change after irradiation at 3×10^{15} cm^{-2}. However, as we will discuss later, the degradation of I_{SC} can occur in certain TJ cells. A similar result was observed for the measurement of I_{SC} at 300 K. By contrast, open-circuit voltage (V_{OC}) values decreased from 3.427 to 3.247 V at 123 K and recovered up to 3.281 V (ΔV = 34 mV) after RT annealing. The recovery of V_{OC} after RT annealing is, however, quite small to contribute to a substantial increase of maximum power (P_{MAX}) of the cell (expected around 1% of contribution to the P_{MAX} recovery). In general, independent of the annealing, V_{OC} degrades more at 300 K than at 123 K. If we consider now the change of fill factor (FF) and P_{MAX}, it is clearly seen that a large change occurred in both LT (123 K) and RT (300 K) measurements. The contribution of FF to the degradation of P_{MAX} is notably higher at 123 K than at 300 K. Moreover, the recovery of P_{MAX} by 20% observed after RT annealing is mainly due to the recovery of FF (18%). This observation

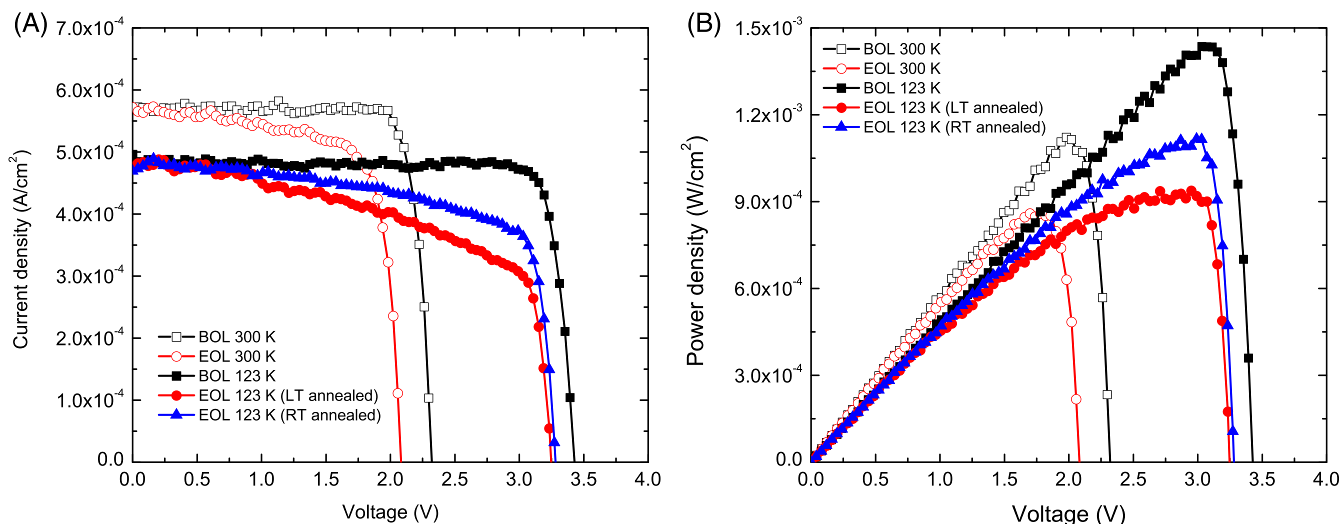

FIGURE 2 Beginning of life (BOL) and end of life (EOL) electrical properties of a triple junction (TJ) solar cell at 123 and 300 K under 0.037 AM0 of illumination (≈ 50.5 W/m^2). 1 MeV irradiation is conducted at 123 K with a fluence of 3 × 1015 cm^{-2}: A, *I-V* curves and B, *P-V* curves [Colour figure can be viewed at wileyonlinelibrary.com]

TABLE 1 Beginning of life (BOL) and end of life (EOL) performance (I_{SC}, V_{OC}, FF, P_{MAX}) of an electron irradiated triple junction (TJ) solar cell

	123 K (LT)			300 K (RT)	
	BOL	EOL LT annealed	EOL RT annealed	BOL	EOL
I_{SC} (mA/cm^2)	0.48	0.48	0.48	0.57	0.57
V_{OC} (mV)	3.427	3.247	3.281	2.321	2.083
FF (%)	86.9	59.8	70.7	85.0	72.7
P_{MAX} (mW/cm^2)	1.44	0.94	1.12	1.12	0.86

Note: Light *I-V* characteristics measured under the solar simulator light intensity of 50 W/m^2, at 123 K (low temperature [LT]) and 300 K (room temperature [RT]); 1 MeV electron irradiation performed at 123 K with a fluence of 3×10^{15} cm^{-2}. The irradiated solar cell annealed at 123 K (LT annealing) and at 300 K (RT annealing).

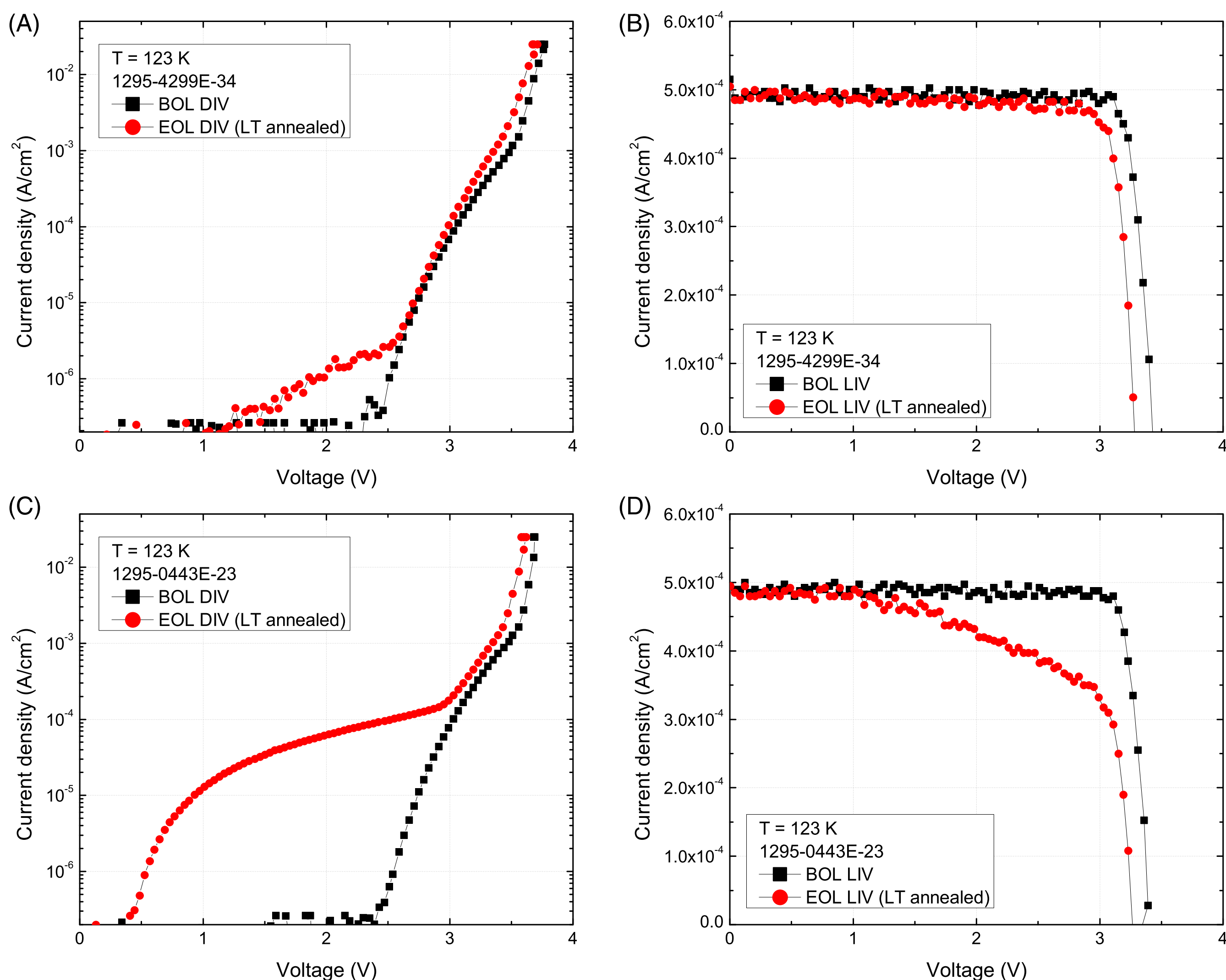

FIGURE 3 Beginning of life (BOL) and end of life (EOL) *I-V* characteristics of two triple junction (TJ) cell in dark (log scale) and under 0.037 AM0 of illumination (≈ 50.5 W/m2) at 123 K: 1295-4299E-34 A and B, and 1295-0443E-23 C and D,, electron irradiated at 123 K with a fluence of 1.5 × 1015 cm^{-2} [Colour figure can be viewed at wileyonlinelibrary.com]

demonstrates that the in situ measurement at 123 K after electron irradiation is essential to correctly measure the performance degradation of cells in LILT conditions.

To investigate the origin of this striking FF deterioration, we compared the LIV and DIV characteristics of two TJ cells, labeled as 1295-4299E-34 and 1295-0443E-23

in Figure 3, which were irradiated with a fluence of 1.5×10^{15} cm^{-2} at 123 K. As shown in Figure 3, these two cells exhibited almost the same BOL performance in both LIV and DIV characteristics. However, once the cells were irradiated, they started to show completely different behavior. In case of the cell 1295-4299E-34, we observed that the EOL dark current started to exceed the current level of 2.5×10^{-7} A/cm^2 from around 1.2 V, then increased up to 2.5×10^{-6} A/cm^2 before it was overlapped by the recombination current component.[32]

This kind of additional current that occurs in the EOL cells compared to the BOL cells is considered as an excess current (or leakage current) in dark. The excess current is a current generated by minority carrier tunneling through radiation-induced defects in the junctions of each sub-cell. The amount of the excess current in the cell 1295-4299E-34 is too low to affect to the degradation of LIV characteristics (see Figure 3B). On the other hand, even though the cell 1295-0443E-23 was also irradiated with a fluence of 1.5×10^{15} cm^{-2}, a significant amount of the excess current was observed in its DIV characteristics as shown in Figure 3C. Unlike cell 1295-4299E-34, this cell exhibited the excess current starting from 0.5 V and its excess current increased almost up to 0.2 mA/cm^2, followed by recombination current up to 3.5 V. Then, diffusion current dominates the dark current after 3.5 V. As a consequence, the EOL LIV curve of the cell 1295-0443E-23 drops from around 1.2 V where the dark current starts to exceed the current of 20 μA/cm^2 (Figure 3D).

In fact, through a number of electron irradiations (48 cells) at three different fluences (7.5×10^{14}, 1.5×10^{15} 3×10^{15} cm^{-2}), we found that the distribution of excess currents in dark covered a range between few 10^{-7} and 10^{-4} A/cm^2 (three orders of magnitude), which had not been observed in proton-irradiated TJ solar cells. Furthermore, FF and thus P_{MAX} degradation was mainly affected by the amount of excess current. Figure 4 shows the relationship between excess current in dark (I_{Dark}) measured at 2 V and P_{MAX} of the TJ cells. All of the cells have been irradiated and measured at 123 K. The cells irradiated with a fluence of 7.5×10^{14} cm^{-2} have P_{MAX} values between 1.4 to 1.5 mW/cm^2 (except for one cell of 1.25 mW/cm^2 with 20 μA/cm^2 of excess current). We can see that the EOL P_{MAX} (black colored squares in Figure 4) was hardly affected by the excess current even though it exceeded 10 μA/cm^2 since the amount of the excess current was still too small compared to the photogenerated current. However, for the cells irradiated with a fluence of 1.5×10^{15} cm^{-2}, we could see a larger spread in P_{MAX} (from 1.03 to 1.45 mW/cm^2). The EOL P_{MAX} values were even more scattered in the case of electron fluence of 3×10^{15} cm^{-2}. The I_{Dark} varied from 2.5 to

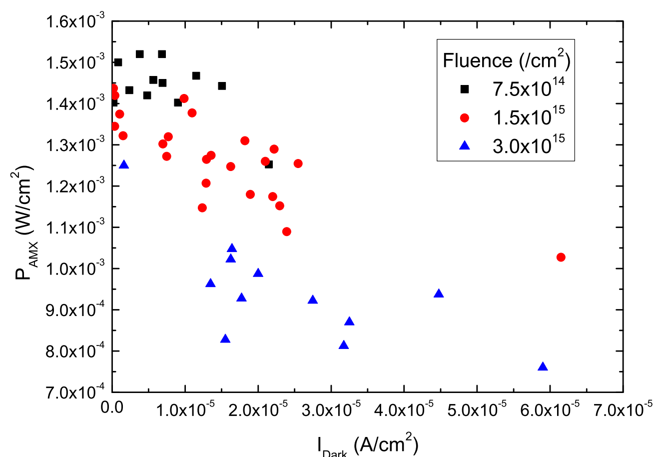

FIGURE 4 Correlation between I_{Dark} at 2 V and P_{MAX} of electron irradiated triple junction (TJ) cells at 123 K. Black square dots, red circles and blue triangles represents the TJ cells irradiated with the fluences of 7.5×1014 cm^{-2}, $1.5 \times 10_{15}$ cm^{-2} and 3.0 $\times$ 1015 cm^{-2}, respectively [Colour figure can be viewed at wileyonlinelibrary.com]

60 μA/cm^2. As a result, the variation of P_{MAX} value was also high from 0.75 to 1.25 mW/cm^2. We found that the degradation of P_{MAX} due to the distortion of the I–V curve starts to be visible from a certain amount of fluence (in case of our study, this was 1.5×10^{15} cm^{-2}) under LILT condition. Furthermore, uncertainty of the EOL performance was increased as we increased the electron fluence.

Figure 5 shows BOL and EOL I-V characteristics in dark and under illumination of TJ cell 1295-0443E-23 at 123 K in linear scale. As shown, the shapes of DIV and LIV curves at BOL and EOL look similar since the solar cell approximately follows the superposition principle. Thus, we can simply assume that the photogenerated current is added to the dark current. An increase of the slope of EOL dark current at around 0.7 V is therefore directly linked to the performance degradation of the TJ cell. Thus, when the excess current in dark increases over 20 μA/cm^2, a non-negligible decrease of the current in the linear scale LIV starts to be observed resulting in a significant degradation of P_{MAX}. Indeed, the BOL and EOL P_{MAX} of TJ cell 1295-0443E-23 are $P_{MAX,\ BOL}$ = 1.5 mW/cm^2 and $P_{MAX,\ EOL}$ = 1.03 mW/cm^2, respectively. If we assume that $P_{MAX,\ EOL}$, is only deduced (assuming no change in the fill factor) from the small I_{SC} and V_{OC} changes after irradiation, corresponding to increased minority carrier recombination due to particle irradiation, it would be of the order of 1.43 mW/cm^2. From this analysis, one can see that the excess current can significantly degrade the performance of the TJ cell at the maximum power operation. According to Reinhardt et al,[33] P_{MAX} is directly related to I_{SC} and the dark

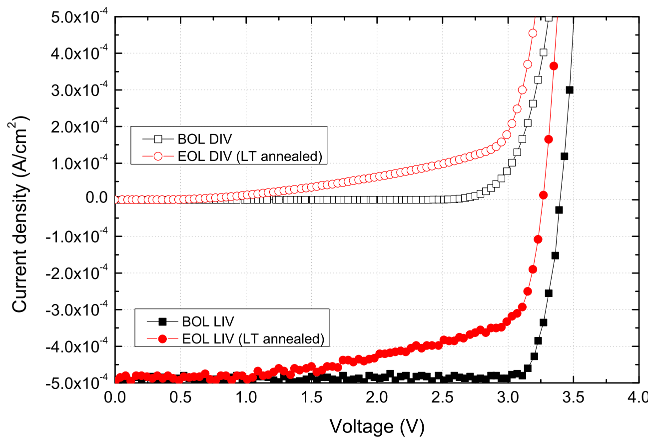

FIGURE 5 Beginning of life (BOL) and end of life (EOL) *I-V* characteristics in dark and under illumination of a 1295-0443E-23 triple junction (TJ) cell at 123 K, irradiated with 1-MeV electrons at 1.5 × 1015 cm^{-2} [Colour figure can be viewed at wileyonlinelibrary.com]

current at maximum power ($I_{d\ MAX}$) through the following relation:

$$P_{MAX} = (I_{SC} - I_{d\ max})\left(\frac{nk_B T}{q}\right)\ln\left(\frac{I_{d\ MAX}}{I_0}\right) \quad (1)$$

where n and I_0 are ideality factor and reverse saturation current, respectively.

The value of ideality factor in the Equation (1) varies as a function of applied voltage because the current generated in solar cell in dark is a mixture of tunneling, diffusion and recombination currents. The contribution of each element to the current depends on the applied voltage level, that is, the applied electrical field in the junction. At low voltage region, for example, high value of ideality factor would indicate dominance of radiation-induced tunneling current. When the ideality factor is large enough, the dark current level (mainly due to the radiation-induced tunneling current) becomes high too.

By this equation, as the cell exhibits higher $I_{d\ MAX}$, its maximum power becomes smaller. Furthermore, the effect of $I_{d\ MAX}$ is especially critical when I_{SC} is sufficiently small like in the LILT deep space conditions where the light intensity is very low. Therefore, the control of this excess current is of prime importance for mastering the degradation since the maximum power is directly related to its value.

For each TJ cell, the photovoltaic parameters such as I_{SC}, V_{OC}, $I_{SC} \times V_{OC}$, FF and P_{MAX} were extracted from both BOL and EOL *I–V* characteristics. Average RF values of each parameter with SD vs fluence are presented in Figure 6.

The electrical parameters of the same cells measured at 300 K are also presented. In addition, data from two TJ cells irradiated at 300 K at different fluences are added for comparison with LT irradiated, but RT measured ones. As one can see, independent of whether the cells are irradiated at LT or at RT, once the cell is measured at RT at the end, the cells exhibit a similar degradation trend. This result implies that when the cell is heated up, it loses its intrinsic behavior which can only be observed at LT. This finding is important for the analysis of irradiation effects in deep space missions, since measuring the *I-V* characteristics of a cell at higher temperature than the temperature where the cell is operated and irradiated can result in a misinterpretation of the cell electrical properties.

At 123 K, when the cells were irradiated with the lowest fluence of 7.5 × 10^{14} cm^{-2}, average I_{SC} value did not change. It seems that the fluences less than about 7.5 × 10^{14} cm^{-2} are too low to create a significant number of defects leading to a dominant decrease of carrier lifetime related to the minority carrier recombination. However, as one can see from the SD of the values, the degradation of I_{SC} varied from cell to cell, which means that there is some variation in the EOL performance. In addition, this spread becomes larger at higher fluences. As to the I_{SC}, it seems that a considerable degradation starts at electron fluences in the range between 7.5 × 10^{14} and 1.5 × 10^{15} cm^{-2}. We could also observe that the cells, which were irradiated with a fluence of about 3 × 10^{15} cm^{-2}, showed in average a larger drop of I_{SC} compared to the case of smaller fluences, suggesting a possible change in current limitation from top to middle cell. On the contrary, the average EOL V_{OC} value was in average degraded down to 96% from its BOL value after the irradiation with a fluence of 7.5 × 10^{14} cm^{-2}, and the overall degradation trend is similar for all cells. Thus, we observe relatively low spread in EOL V_{OC} values compared to the case of I_{SC}. Besides the degradation of I_{SC} and V_{OC}, the degradation of P_{MAX} appears larger than the product $I_{SC} \times V_{OC}$ (see Figure 6B), which implies that an additional phenomenon, other than the recombination of photo-carriers on the defects,[34,35] participates to the degradation. Owing to the large scatter of this effect induced on P_{MAX} and on FF, the amount of EOL excess current seems to be directly related to P_{MAX} degradation. Similarly, a significant, but lesser spread of EOL P_{MAX} was recently obtained from full size cells (4 cm × 8 cm) in LILT 1-MeV electron irradiation conditions by Duzellier et al.[30] The averaging effect on a larger cell can be one potential reason why we see less spread, but it could be confirmed only if the identical experiment is repeated on the same type of large samples at the SIRIUS facility. However, when the cells are measured at 300 K, they

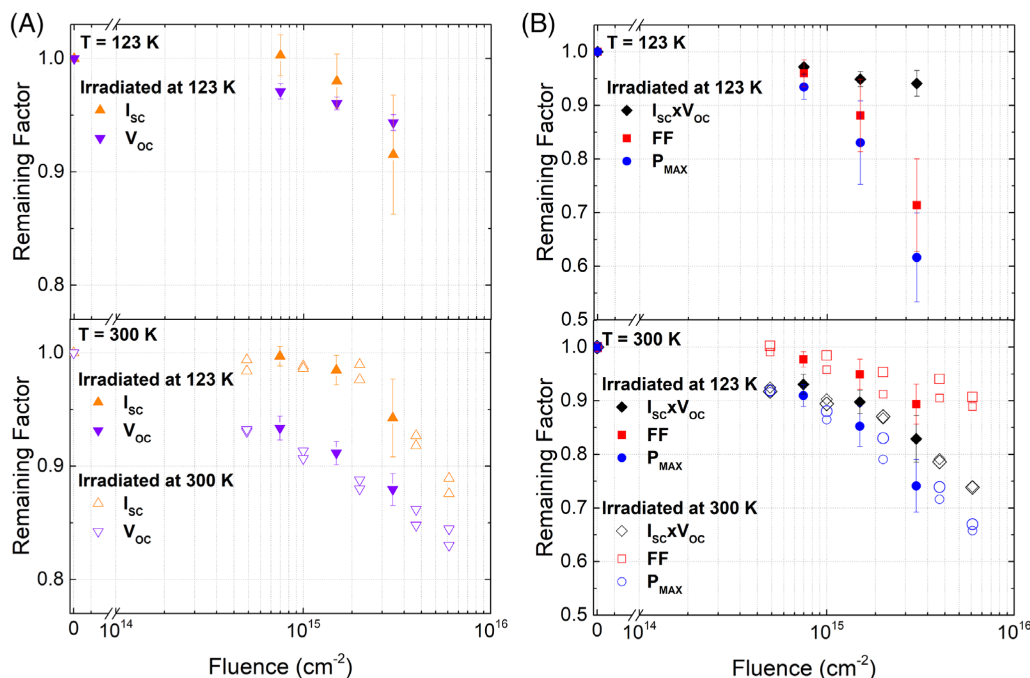

FIGURE 6 Remaining factor of A, I_{SC}, V_{OC} and B, $I_{SC} \times VOC$, FF, *PMAX* of triple junction (TJ) solar cells at 123 and 300 K. The number of solar cells irradiated at 123 K: 12 cells at 7.5 × 1014 cm^{-2}, 24 cells at 1.5 × 1015 cm^{-2}, 12 cells at 3 × 1015 cm^{-2}. The number of solar cells irradiated at 300 K: 2 cells with accumulated fluences from 5 × 1014 cm^{-2} to 6 × 1015 cm^{-2} [Colour figure can be viewed at wileyonlinelibrary.com]

behave differently. As to V_{OC}, the rate of degradation becomes higher at 300 K compared to 123 K. For FF, the degradation at 300 K is smaller than the one observed at 123 K, and it exhibits a smaller scatter. The overall degradation of P_{MAX} under electron irradiation at 123 K, measured at 300 K remains smaller than the one observed at continuous low temperature conditions. In addition, once the temperature of the TJ cells was increased to 300 K after the irradiation at 123 K, their electrical performance was very similar to this one of the cells irradiated at 300 K.

3.2 | Excess current in component cells

The appearance of an excess current, following electron irradiation at low temperatures, was also observed in all component cells (see Figure 7). In general, before irradiation the bottom component cell exhibits a three to four orders of magnitude higher dark current than the two component cells. Note that in an ideal situation, no net current flows in solar cell in dark at thermal equilibrium. The BOL dark current of a bottom cell is about 2.5 x 10^{-7} A/cm^2 at voltage close to 0 V and increased up to more than 2.5 x 10^{-5} A/cm^2 before the diffusion current starts to exponentially increase. When the bottom cell was irradiated with a fluence of 3×10^{15} cm^{-2}, the EOL dark current was one order of magnitude larger than the BOL value while the degradation of the diffusion current was relatively small. As to the top and middle component cells, BOL dark current was at the level of 10^{-10} A/cm^2 at voltage close to 0 V, then the current increased up to 10^{-8} A/cm^2 before the diffusion current dominated the current in dark. The degradation of diffusion current

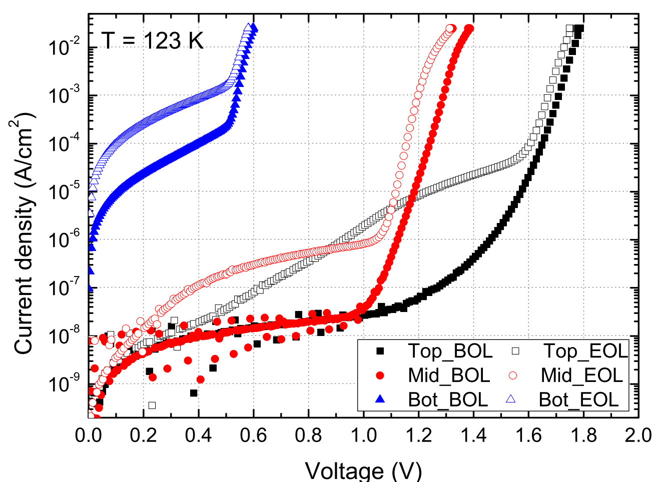

FIGURE 7 *I-V* characteristics of component cells in dark before and after electron irradiation with a fluence of 3 × 1015 cm^{-2} at 123 K [Colour figure can be viewed at wileyonlinelibrary.com]

could result from the radiation-induced defects acting as recombination centers. According to the study by Tex et al, in both electron-irradiated GaInP and GaAs sub-cells nonradiative recombination losses were observed.[36] When comparing the EOL properties of top and middle cells in dark, a larger degradation of diffusion current of the middle cell was observed in comparison to that of the top cell. However, the excess current of the top cell increased over 10^{-5} A/cm^2 where it can affect the P_{MAX} degradation whereas that of the middle cell was under 10^{-6} A/cm^2. Overall, this observation shows that any sub-cell can potentially be the cause of the degradation of FF of TJ cells in LILT conditions.

We also investigated the temperature dependence of the DIV of electron irradiated bottom component cells. Figure 8 presents DIV measurements performed at temperatures ranging from 123 to 300 K after irradiation at 123 K (pre and post annealing at 300 K). The excess current seems to be temperature independent while heating up. After the bottom cell temperature reached 300 K, the bottom cell was again cooled down from 300 to 123 K with intermediate measurements (see the symbols with no fill color). We observed a diminution of the excess current as temperature decreased. Eventually, the RT annealed bottom cell exhibited about one order smaller amount of excess current in dark at 123 K compared to the case before annealing.

Similar observation was obtained for top and middle component cells when cooling down from 300 to 100 K as shown in Figure 9. The excess current is smaller at the same working voltages when the cell is measured at lower temperatures. The shape of excess current in top cell seems to be more complicated than that of the middle one. The prediction of the exact value and the shape of the excess current characteristic seems to be quite

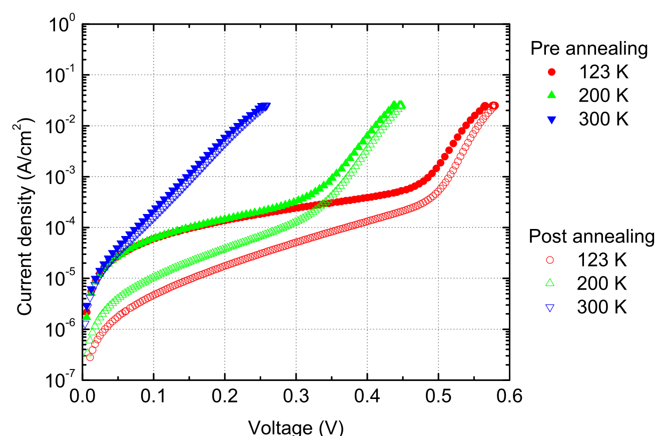

FIGURE 8 End of life (EOL) *I-V* characteristics of a bottom component cell electron irradiated at 123 K with a fluence of 3×1015 cm^{-2}: pre and postannealing at 300 K [Colour figure can be viewed at wileyonlinelibrary.com]

challenging since it really appears with various forms from cell to cell and there could be other kinds of unknown contributions. For some cells no additional excess current has been observed. More detailed research should be undertaken, but it seems to be also related to the manufacturing-related variations of microscopic cell structure.

3.3 | Annealing

We carried out isochronal annealing of the top and bottom cells. The isochronal annealing is the annealing performed with the temperature increase in the constant temperature step and with the same annealing time at each temperature step. We discarded middle cells because it is known that the defects induced in GaAs by electron irradiation remain stable in the range 4 to 350 K.[7] The cells used for this procedure were irradiated at 96 K with a fluence of 1×10^{15} cm^{-2}. Figure 10A,B shows the changes of the remaining factors (RF) of I_{SC}, V_{OC}, P_{MAX}, FF of top and bottom cells, respectively, as a function of annealing temperature. (RF(Z) = EOL(Z)/BOL(Z), Z is an electrical parameter, for example, I_{SC} or V_{OC}).

In the top cell, the degradation of V_{OC} was small (1%-2%) compared to other parameters such as I_{SC} and FF, and nearly no recovery was observed. The recovery of I_{SC} was also not evident during the isochronal annealing, and the RF(I_{SC}) after RT annealing was only increased by 2%. The FF recovery seems to be stronger than the case of I_{SC}. However, RF(FF) was recovered by 4% after RT annealing. As a result, P_{MAX} recovered by only about 6%. For the bottom cell, it exhibited somewhat different behaviors. First, the degradation of V_{OC} was quite pronounced. RF(V_{OC}) decreased to 0.25 immediately after the irradiation. Then, RF(V_{OC}) recovered from 0.25 to 0.5 in 5 minutes. After the first huge recovery at the irradiating temperature (96 K), we could measure a steady recovery of V_{OC} in the range between 116 and 240 K, having smaller recovery rate as temperature increases. Second, the I_{SC} value decreased significantly after irradiation, whereas two step-like annealing stages of RF(I_{SC}) were observed, around 100 and 200 K. The recovery of FF was not remarkable compared to that of V_{OC}. Nevertheless, RF(FF) also dropped notably and recovered quickly from 0.77 up to 0.84 at the irradiated temperature (96 K). Then, like in the case of V_{OC}, a gradual recovery was observed up to 0.9 at the temperature ranging from 96 to 200 K. Above 200 K, no further FF recovery was measured. Consequently, P_{MAX} of the bottom cell decreased down to 10% of its BOL value after the irradiation due to the large degradation of I_{SC} and V_{OC}. However, the P_{MAX}

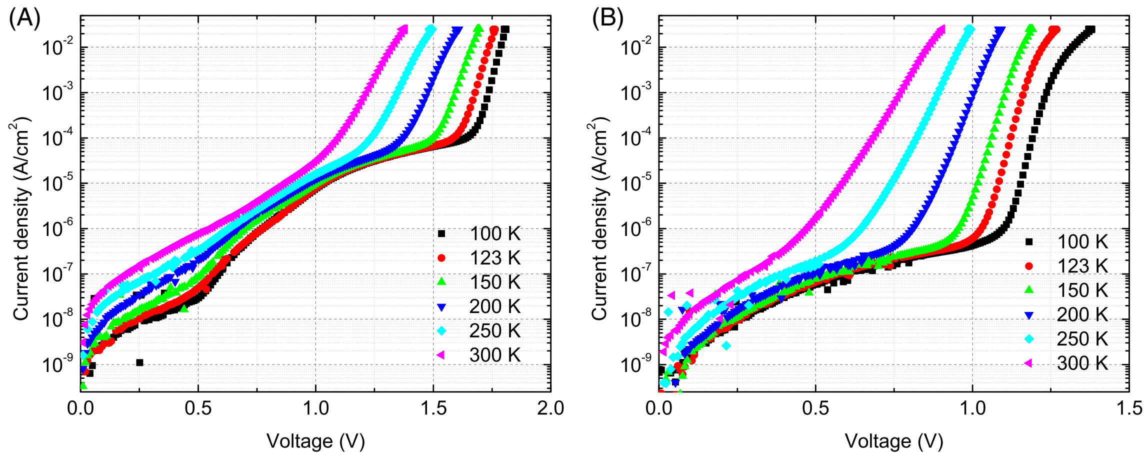

FIGURE 9 *I-V* characteristics of electron irradiated A, top and B, middle component cells in dark for temperatures ranging from 300 to 100 K. The cells were irradiated at 123 K with a fluence of 3 × 1015 cm^{-2} [Colour figure can be viewed at wileyonlinelibrary.com]

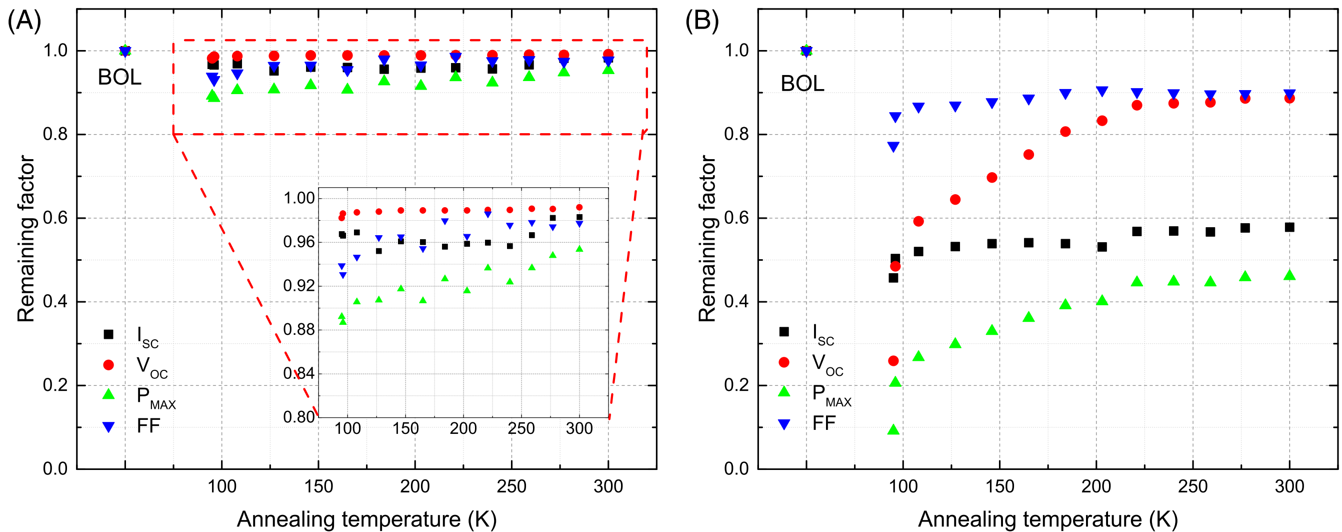

FIGURE 10 Change of I_{SC}, V_{OC}, P_{MAX}, FF Remaining factors of electron irradiated cells with a fluence of 1 × 1015 cm^{-2} at 96 K. A, top and B, bottom component cells during isochronal annealing (96 K was the lowest temperature that could be achieved with the used set up) [Colour figure can be viewed at wileyonlinelibrary.com]

regained its performance ending up in a value of 0.5 of RF(P_{MAX}), mainly related to the V_{OC} recovery.

4 | DISCUSSION

4.1 | Origin of the excess current

We analyzed the excess current observed after LT irradiation in detail to understand its physical cause. As presented in Figure 8 for the bottom cell, we can assume that some defects induced by electron irradiation are annealed out, resulting in a recovery of excess and diffusion currents. In fact, the excess current consists of several components which is complicated to analyze. The defects linked to the excess current act as localized traps in space charge region of a p-n junction, where the majority charge carriers (either electrons or holes) can pass by indirect tunneling mechanism. The excess current related to the radiation-induced impurity states in the forbidden gap was already observed by D. Meyerhofer et al.[37] This current is labeled as an exponential excess current. Chynoweth et al[38] proposed the equation of the exponential excess current which depends on the doping and the bombardment as below:

$$J_{\text{exc}} = D' \exp\left[-\beta' m^{*\frac{1}{2}} n^{*-\frac{1}{2}} (E_G - eV + Q)\right] \tag{2}$$

where D' is the function of V, which is dependent of temperature and represents the variation of the density of

impurity states with energy in the forbidden gap, m^* is a reduced mass of electron, n^* is a reduced doping concentration, Q is a function of the sum of the Fermi level penetrations, and E_G is a bandgap energy.

As described, the excess current is different from the band-to-band tunneling, but still has a tunneling feature through impurity states (traps) in the forbidden gap. However, this excess current shows temperature-dependent properties. A simple diagram in Figure 11 illustrates trap-assisted tunneling (TAT) of an electron from the conduction band of the n-doped side to the valence band of p-doped side in the junction. This excess current is proportional to the density of occupied states in the conduction band. Therefore, a possible explanation of its temperature dependence is that the density of occupied states with electrons in the conduction band will decrease resulting in the reduced amount of excess current at lower temperatures. In addition, the tunneling probability can be dependent on the concentration and the trap level of defects located in the space charge region. Especially, the TAT current can more easily appear in Ge bottom cells than in other cells since the Ge has a narrower bandgap compared to GaAs and GaInP. Likewise, the internal electric field, which causes a band bending between n-doped and p-doped layers, can play an important role to the dark current. When the external field with positive bias is applied to the pn junction, the sum of two fields will result in diminution of the bending of the junction. Consequently, more carriers in occupied states in the conduction band will be able to travel to the valance band via trap states in the forbidden gap.

4.2 | Ge bottom cell—electron and proton irradiations at LILT condition

Under electron and proton irradiation at LILT condition, the most complex behavior has been mostly observed in bottom cells. When the bottom cells are irradiated with protons, they undergo a drastic I_{SC} degradation and eventually can become the current limiting cell below 200 K. However, proton-irradiated bottom cells do not exhibit an additional excess current in dark. (for more detail, see the Ref. 20) The behavior of electron-irradiated cells is rather different. First, a large amount of excess current in dark is added after electron irradiation. Second, we observe relatively little degradation of I_{SC} in an electron-irradiated bottom cell compared to the proton irradiated one. Thus, there is practically no possibility for the bottom cell to be a current limiting cell in a purely electron dominated environment. This observation can be tentatively explained by a distribution model of radiation-induced defects. Electrons transfer energy to the lattice atoms of the order of the threshold displacement energy (T_d), so that they produce mostly single displacements along their track. As a result, they create a uniform distribution of isolated defects.

If irradiation-induced defects have enough mobility to escape the region where they have been produced to be uniformly distributed like in the case for Si (vacancies are mobile above 100 K[39]), the damage factor ratios should be directly proportional to the nonionizing energy loss (NIEL) for electrons and protons.[40] This is not the case for defects induced by proton irradiation at lower temperatures in Ge, where a large number of displacements is produced along the proton track and the associated defects are not mobile enough. It results in a high local concentration of defects composed of complexes such as divacancies which are stable and charged.[20]

4.3 | Annealing: defects and the excess current

Radiation-induced defects can contribute to the degradation of solar cells in different ways: (a) acting as

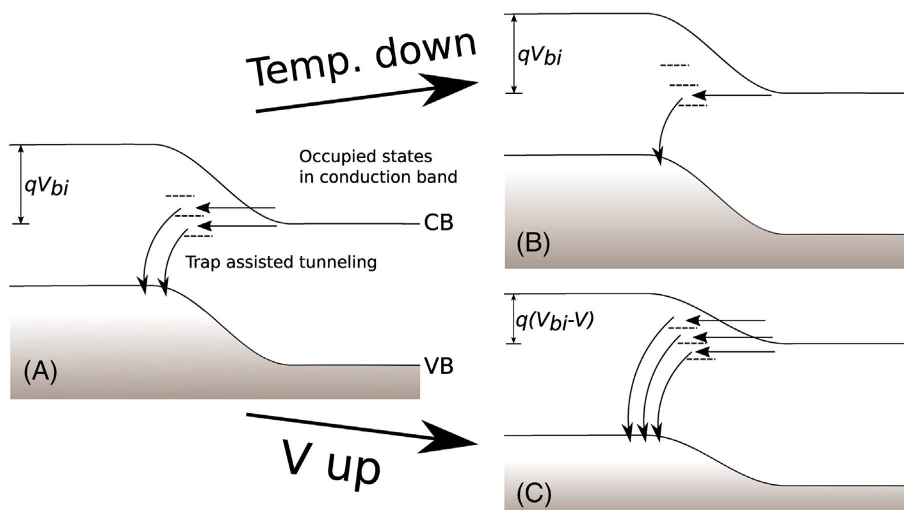

FIGURE 11 Simplified band diagram of Ge pn junction with localized trap levels induced by electron irradiation: A, thermal equilibrium state ($V = 0$); B, thermal equilibrium at low temperature (LT); C, positive biased ($V > 0$) [Colour figure can be viewed at wileyonlinelibrary.com]

recombination centers in n-type and p-type layers or in the depletion region. In this case, the result is observed as a diminution of photo-generated current, an increase of dark diffusion current and recombination current which are directly correlated to V_{OC}. (b) In case of very large fluence, compensating centers to reduce a doping effect in each doped layer. The associated defects result in a degradation of both V_{OC} and I_{SC}.[41] (c) Indirect tunneling centers for the majority carriers. They can play a role as an intermediate pathway of electrons or holes so that these carriers can pass through the forbidden band. Consequently, higher excess current can flow in dark before the diffusion current starts to dominate the dark current.

In a TJ cell, LIV characteristics are significantly affected by the current limiting sub-cell. Moreover, if this current limiting sub-cell exhibits a large enough excess current, the TJ cell immediately shows a deterioration of FF followed by P_{MAX} degradation. Depending on the operating voltage, it can be due to any sub-cell among top, middle and bottom cells.

In GaAs, primary defects in arsenic sublattice ($V_{As} - As_i$) and As_{Ga} antisite related defects are mainly generated by MeV electron irradiation. However, these defects are not only associated with one trap level, rather they appear to be on many different levels between the conduction and the valence bands.[7,42-44] It is also known that the defects induced in GaAs by MeV electron irradiation remain stable in the range 4 to 350 K.[7] Thus, it seems reasonable that the TAT happens via one or more trap levels associated with described defects which are not recovered in the range between 120 and 300 K.

In the case of radiation-induced defects in GaInP, information in the literature is still missing. There have been reports on the primary defects in phosphorus sublattice ($V_P - P_i$) with trap levels close to the valence band and some complexes with impurities or secondary defects which create trap levels close to the conduction band.[45] These defects can be measured under the room temperature, and we have not observed any particular recovery stage except for a few percent in FF (so as in P_{MAX}) from the annealing test of the top cell. This result implies that there could exist still unidentified defects that are involved in the TAT and have annealing temperatures (T_a) below 300 K. To master the knowledge of defects in GaInP, more quantitative analysis will be necessary. Based on the performed studies, we can conclude that the top and middle sub-cells do not cause critical difference even when they are irradiated at RT and measured at LT because their radiation-induced defects are mostly stable in the temperature range between 120 and 300 K except some small effects on FF. In other words, the excess current can still occur in a TJ cell by RT irradiation, originated from the top or the middle cell.

Meanwhile, it is known that the kinetics of radiation-induced defects in Ge is more dynamic. The interstitial states are mobile above 65 K, and the vacancies become mobile at 100 K.[46] Furthermore, nearly 95% of defects disappear at 65 K.[47] Namely, the behavior of electron-irradiated Ge cell at LILT condition is governed by less than 5% of radiation-induced defects. The subsequent recovery of I_{SC} at 100 and 200 K is consistent with defect annealing studies in n-type Ge. Recovery at 100 K seems to stem from annealing of vacancy related defects and in succession, at 200 K can be from annealing of A-centers (vacancy − oxygen complex),[48] germanium self-interstitials (Ge_i) and vacancies.[19] Furthermore, in p-type Ge, the single vacancy and the gallium interstitial (Ga_i) can be good candidates because both disappeared after room temperature annealing.[19]

Apart from the recovery of I_{SC}, we could also remark that the excess current in dark, that is, the TAT current was recovered. According to the extensive study by Fage-Pedersen et al,[49] most of defects induced by electron and proton irradiations are identical except the divacancy. Furthermore, the most remarkable difference between the electron and proton-irradiated Ge cells is the occurrence of excess current which in subsequence, resulting in a large degradation of FF and V_{OC}. Therefore, it can be supposed that its annealing behavior at LT and RT can be directly related to the secondary defects like divacancies.

5 | CONCLUSION

When irradiating TJ solar cells with 1 MeV electrons at low temperatures, we observed a severe degradation of FF at higher fluences which was not observed in our proton study.[16] This FF degradation is due to the high excess current which can be measured in dark and this appears larger at low temperatures. The excess current in dark originates from trap-assisted indirect tunneling, mainly from the bottom cell, a little extend from the top cell and a lesser from the middle cell. The bottom cell degraded the most after the electron irradiation at low temperature, but also largely recovered after LT and RT annealing due to its dynamic kinetic of radiation induced defects under room temperature. The trap-assisted tunneling seems to be induced by primary defects (Frenkel pairs) and secondary defects in the top and the middle cells and by divacancies in the bottom cell. A significant spread in P_{MAX} degradation of 2 cm × 2 cm 3G28 TJ cells was observed in the electron irradiation condition. We attribute this to manufacturing-related microscopic inhomogeneities in the TJ cell structure (not electrically measurable), which can induce defects upon

irradiation. It is expected that the spread (uncertainty) of EOL P_{MAX} performance can be diminished in full-size TJ cells thanks to the averaging effect on a larger cell. In order to confirm it, an extensive round robin irradiation tests not only with 2 cm x 2 cm size cells but also with the full-size cells would be required to evaluate several space-qualified solar cells (eg, Spectrolab UTJ, SolAero ZTJ and Azurspace 3G28-LILT) that have different cell technologies at different irradiation facilities that are capable of performing in situ LILT measurement following LT irradiation. It is expected to be realized in the near future.[50]

Suppressing the excess current of sub-cells in dark is the way to improve TJ cell performance at LILT electron irradiation conditions since the P_{MAX} is directly related to its amplitude. Further study will be required to better understand the dependence of the excess current on the cell structure.

ACKNOWLEDGEMENTS

The present work was supported by the European Space Agency under contract no. 4000109645. The irradiation has been performed at the SIRIUS facility of Laboratoire des Solides Irradiées and supported by EMIR federation (EMIR project no. 15-5727). We gratefully thank to Prof. Jacques Bourgoin for valuable and constructive discussions and his support in the interpretation of obtained results.

DATA AVAILABILITY STATEMENT

The data that support the findings of this study are available from the corresponding author upon reasonable request.

REFERENCES

1. Corbett JW, Bourgoin JC, Weigel C. Radiation damage and defects in semiconductors. London: The Institute of Physics; 1973.
2. Emtsev V. Point defects in germanium: reliable and questionable data in radiation experiments. *Mater Sci Semicond Process*. 2006;9(4):580-588. https://doi.org/10.1016/j.mssp.2006.08.074.
3. Zazoui M, Bourgoin JC, Deresmes D, et al. Recombination centers in electron-irradiated Czochralski silicon solar cells. *J Appl Phys*. 1994;76(2):815-819. https://doi.org/10.1063/1.357755.
4. Bourgoin J, Lannoo M. *Point Defects in Semiconductors II. Vol. 35*. Berlin, Heidelberg: Springer; 1983. doi:https://doi.org/10.1007/978-3-642-81832-5.
5. Srour JR, Marshall CJ, Marshall PW. Review of displacement damage effects in silicon devices. *IEEE Trans Nucl Sci*. 2003;50(3):653-670. https://doi.org/10.1109/TNS.2003.813197.
6. Newman RC. Defects in silicon. *Rep Prog Phys*. 2000;45(10):1163-1210. https://doi.org/10.1088/0034-4885/45/10/003.
7. Pons D, Bourgoin JC. Irradiation-induced defects in GaAs. *J Phys C: Solid State Phys*. 1985;18(20):3839-3871. https://doi.org/10.1088/0022-3719/18/20/012.
8. Danilchenko B, Danilchenko B, Budnyk A, et al. 1MeV electron irradiation influence on GaAs solar cell performance. *Sol Energy Mater Sol Cells*. 2008;92(11):1336-1340. https://doi.org/10.1016/j.solmat.2008.05.006.
9. Khan A, Khan A, Yamaguchi M, et al. Recombination centers in electron irradiated GaInP: application to the degradation of space solar cells. *J Cryst Growth*. 2000;210(1–3):264-267. https://doi.org/10.1016/s0022-0248(99)00693-4.
10. Dekker J, Oila J, Saarinen K, Tukiainen A, Li W, Pessa M. Cation and anion vacancies in proton irradiated GaInP. *J Appl Phys*. 2002;92(10):5942-5949. https://doi.org/10.1063/1.1515123.
11. Zaidi MA, Zazoui M, Bourgoin JC. Defects in electron irradiated GaInP. *J Appl Phys*. 1993;73(11):7229-7231. https://doi.org/10.1063/1.354009.
12. Okuno Y, Okuda S, Akiyoshi M, et al. Radiation degradation prediction for InGaP solar cells by using appropriate estimation method for displacement threshold energy. *J Appl Phys*. 2017;122(11):114901-114908. https://doi.org/10.1063/1.4989891.
13. Mooney PM, Cherki M, Bourgoin JC. Energy levels in electron irradiated n-type germanium. *J Physique Lett*. 1979;40(2):19-22. https://doi.org/10.1051/jphyslet:0197900400201900.
14. Elsayed M, Arutyunov NY, Krause-Rehberg R, Oganesyan GA, Kozlovski VV. Formation and annealing of vacancy-P complexes in proton-irradiated germanium. *Acta Mater*. 2015;100(C):1-10. https://doi.org/10.1016/j.actamat.2015.08.039.
15. Tada HY, Carter JRJ, Anspaugh BE, Downing RG. *Solar Cell Radiation Handbook*. Pasadena, CA: JPL Publication; 1982 https://ntrs.nasa.gov/search.jsp?R=19830006416.
16. Whitehouse JE. Electron irradiation of p-type germanium at 4.2°K. *Phys Rev*. 1966;143(2):520-525. https://doi.org/10.1103/PhysRev.143.520.
17. Bourgoin J, Mollot F. Behaviour of primary defects in electron-irradiated germanium. *Phys Status Solidi (b)*. 1971;43(1):343-355. https://doi.org/10.1002/pssb.2220430136.
18. Mooney PM, Poulin F, Bourgoin JC. Annealing of electron-induced defects in n-type germanium. *Phys Rev B*. 1983;28(6):3372-3377. https://doi.org/10.1103/PhysRevB.28.3372.
19. Mesli A, Dobaczewski L, Nielsen KB, Kolkovsky V, Petersen MC, Larsen AN. Low-temperature irradiation-induced defects in germanium: in situ analysis. *Phys Rev B Condens Matter Mater Phys*. 2008;78(16):165202. https://doi.org/10.1103/PhysRevB.78.165202.
20. Park S, Bourgoin JC, Sim H, et al. Space degradation of 3J solar cells: I-proton irradiation. *Prog Photovolt Res Appl*. 2018;23(1):1-788. https://doi.org/10.1002/pip.3016.
21. Imaizumi M, Takamoto T, Sumita T. Study of radiation response on single-junction component sub-cells in triple-junction solar cells. *The Third World Conference on Photovoltaic Solar Energy Conversion*. Osaka, Japan: IEEE; 2003:599-602.
22. Xin G, Zhan-zu F, Xin-yu C, Sheng-sheng Y, Lei Z. Performance evaluation and prediction of single-junction and triple-junction GaAs solar cells induced by electron and proton irradiations. *IEEE Trans Nucl Sci*. 2014;61(4):1838-1842. https://doi.org/10.1109/TNS.2014.2306991.
23. Hoheisel R, Scheiman D, Messenger S, Jenkins P, Walters R. Detailed characterization of the radiation response of multi-junction solar cells using electroluminescence measurements. *IEEE Trans Nucl Sci*. 2016;62(6):2894-2898. https://doi.org/10.1109/TNS.2015.2498838.

24. Stella P, Davis G, Mueller R, Distefano S. The environmental performance at low intensity, low temperature (LILT) of high efficiency triple junction solar cells. *2nd International Energy Conversion Engineering Conference*. Reston, VA: AIAA (American Institute of Aeronautics and Astronautics); 2004. https://doi.org/10.2514/6.2004–5579.
25. Harris RD, Imaizumi M, Walters RJ, et al. In situ irradiation and measurement of triple junction solar cells at low intensity, low temperature (LILT) conditions. *IEEE Trans Nucl Sci*. 2008; 55(6):3502-3507. https://doi.org/10.1109/TNS.2008.2006971.
26. Baur C, Khorenko V, Siefer G, et al. Development status of triple-junction solar cells optimized for low intensity low temperature applications. *IEEE 39th Photovoltaic Specialists Conference (PVSC)*. Tampa, FL, USA: IEEE; 2013:3237-3242. https://doi.org/10.1109/pvsc.2013.6745142.
27. Bourgoin JC, Boizot B, Khirouni K, Khorenko V. On the prediction of solar cell degradation in space. *10th European Space Power Conference (ESPC)*. Vol. 719. Noordwijk, The Netherlands: ESA communications; 2014:1.
28. Taylor S, Baur C, Torunski T, et al. Performance of European triple-junction solar cells for deep space missions. *Proceedings of the Eighth European Space Power Conference*. Vol. 661. Noordwijk, The Netherlands: ESA communications; 2008:34-39.
29. Park S, Bourgoin JC, Cavani O, Khorenko V, Baur C, Boizot B. Origin of the degradation of triple junction solar cells at low temperature. In: Fernandez A, ed. *E3S Web Conf*. Vol. 16, No. 1. France: EDP Sciences; 2017:04004. https://doi.org/10.1051/e3sconf/20171604004.
30. Duzellier S, Nuns T, David JP, et al. Evaluation of tri-junction solar cells response to electrons and protons of the JUICE specific environment. *2018 IEEE 7th World Conference on Photovoltaic Energy Conversion (WCPEC) (A Joint Conference of 45th IEEE PVSC, 28th PVSEC & 34th EU PVSEC)*. 2018;3329-3334.
31. Khorenko V, Baur C, Siefer G, et al. BOL and EOL characterization of Azur 3G lilt solar cells for ESA juice mission. In: Fernandez A, ed. *E3S Web Conf*. Vol. 16, No. 8. France: EDP Sciences; 2017:03011-03015. https://doi.org/10.1051/e3sconf/20171603011.
32. Sah CT, Noyce RN, Shockley W. Carrier generation and recombination in P-N junctions and P-N junction characteristics. *Proc IRE*. 1957;45(9):1228-1243. https://doi.org/10.1109/JRPROC.1957.278528.
33. Reinhardt KC, Mayberry CS, Lewis BP, Kreifels TL. Multi-junction solar cell iso-junction dark current study. *28th IEEE Photovoltaic Specialists Conference—2000 (Cat No00CH37036)*. Anchorage, AK, USA: IEEE; 2000:1118-1121. https://doi.org/10.1109/pvsc.2000.916083.
34. Zaidi MA, Bourgoin JC, Maaref H. Poole-Frenkel-assisted emission from deep levels in electron-irradiated germanium. *Semicond Sci Technol*. 1989;4(9):739-742. https://doi.org/10.1088/0268-1242/4/9/006.
35. Vincent G, Chantre A, Bois D. Electric field effect on the thermal emission of traps in semiconductor junctions. *J Appl Phys*. 1979;50(8):5484-5487. https://doi.org/10.1063/1.326601.
36. Tex DM, Nakamura T, Imaizumi M, Ohshima T, Kanemitsu Y. Direct evaluation of influence of electron damage on the subcell performance in triple-junction solar cells using photoluminescence decays. *Sci Rep*. 2017;7(1):510. https://doi.org/10.1038/s41598-017-02141-0.
37. Meyerhofer D, Brown GA, Sommers HS. Degenerate germanium. I. Tunnel, excess, and thermal current in tunnel diodes. *Phys Rev*. 1962;126(4):1329-1341. https://doi.org/10.1103/physrev.126.1329.
38. Chynoweth AG, Feldmann WL, Logan RA. Excess tunnel current in silicon Esaki junctions. *Phys Rev*. 1961;121(3):684-694. https://doi.org/10.1103/PhysRev.121.684.
39. Corbett JW, Chang LJ, Lee YH, et al. *The Status of Defect Studies in Silicon*. United Kingdom: Institute of Physics; 1976.
40. Burke EA. Energy dependence of proton-induced displacement damage in silicon. *IEEE Trans Nucl Sci*. 1986;33(6):1276-1281. https://doi.org/10.1109/TNS.1986.4334592.
41. Bourgoin JC, de Angelis N. Radiation-induced defects in solar cell materials. *Sol Energy Mater Sol Cells*. 2001;66(1–4):467-477. https://doi.org/10.1016/s0927-0248(00)00208-7.
42. Lang DV, Kimerling LC. Observation of recombination-enhanced defect reactions in semiconductors. *Phys Rev Lett*. 1974;33(8):489-492. https://doi.org/10.1103/PhysRevLett.33.489.
43. Pons D, Mircea A, Bourgoin J. An annealing study of electron irradiation-induced defects in GaAs. *J Appl Phys*. 1980;51(8): 4150-4157. https://doi.org/10.1063/1.328235.
44. Stievenard D, Bourgoin JC. Defect-enhanced annealing by carrier recombination in GaAs. *Phys Rev B*. 1986;33(12):8410-8415. https://doi.org/10.1103/PhysRevB.33.8410.
45. Khan A, Yamaguchi M, Bourgoin JC, Bourgoin JC, Takamoto T. Thermal annealing study of 1 MeV electron-irradiation-induced defects in n+p InGaP diodes and solar cells. *J Appl Phys*. 2002; 91(4):2391-2397. https://doi.org/10.1063/1.1433936.
46. Whan RE. Investigations of oxygen-defect interactions between 25 and 700°K in irradiated germanium. *Phys Rev*. 1965;140 (2A):A690-A698. https://doi.org/10.1103/PhysRev.140.A690.
47. Callcott TA, Mackay JW. Irradiation damage in n-type germanium at 4.2°K. *Phys Rev*. 1967;161(3):698-710. https://doi.org/10.1103/PhysRev.161.698.
48. Bourgoin JC, Mooney PM, Poulin F. In: Hasiguti RR, ed. *Defects and Radiation Effects in Semiconductors*. Vol 59. Bristol, UK: Institute of Physics; 1980:33.
49. Fage-Pedersen J, Larsen AN, Mesli A. Irradiation-induced defects in Ge studied by transient spectroscopies. *Phys Rev B*. 2000;62(15):10116-10125. https://doi.org/10.1103/PhysRevB.62.10116.
50. Boca A. Solar cell testing for the Jupiter environment: low irradiance, low temperature and high radiation. *IEEE 46th Photovoltaic Specialists Conference (PVSC)*. Chicago, IL, USA: IEEE; 2020. https://doi.org/10.1109/PVSC40753.2019.8981342.

SUPPORTING INFORMATION

Additional supporting information may be found online in the Supporting Information section at the end of this article.

How to cite this article: Park S, Cavani O, Lefèvre J, Baur C, Khorenko V, Boizot B. Space degradation of triple junction solar cells at low temperatures: II-electron irradiation. *Int J Energy Res*. 2021;1-13. https://doi.org/10.1002/er.6937